IEEE Access
Multidisciplinary | Rapid Review | Open Access Journal

Received September 21, 2019, accepted October 15, 2019, date of publication October 21, 2019, date of current version November 1, 2019.

*Digital Object Identifier 10.1109/ACCESS.2019.2948731*

# Study on Reciprocal Models for Magneto-Acousto-Electrical Tomography With Coil Detection

**LIKUN GONG[1], LAN YANG[1], SIYI YANG[1], YUANZE WANG[1], MINJING ZHONG[1], AND LIANG GUO[2], (Member IEEE)**

[1]College of Information and Control Engineering, China University of Petroleum, Qingdao 266580, China
[2]College of Control Science and Engineering, China University of Petroleum, Qingdao 266580, China

Corresponding author: Liang Guo (guoliang@upc.edu.cn)

This work was supported in part by the Qingdao Source Innovation Program under Grant 19-6-2-60-cg, and in part by the Fundamental Research Funds for the Central Universities under Grant 18CX02111A.

**ABSTRACT** Magneto-Acousto-Electric Tomography with coil detection, known as Magneto-Acousto-Electric Tomography with Magnetic Induction (MAET-MI), is a non-contact resistivity-based imaging method that employs a coil to detect the induced current generated by the ultrasound in biological tissue, which lie under a static magnetic field. To reconstruct an image of the tissue's conductivity, we propose a reciprocal model to describe the relationship between the inducted voltage of a coil and its conductivity. Previous work on the reciprocal theorem demonstrates that reconstructing conductivity using this method is effective. The forward and inverse problem are usually not verified both numerically and experimentally. In this paper, different approaches are adopted to calculate the forward and the inverse problems for verification of the reciprocal model. This verifies that the reconstruction method based on electrode detection can be applied to MAET-MI. This means that the inverse problem of MAET-MI can be transformed into an inverse source reconstruction of a wave equation based on the coil detection. In the forward problem, the moment method is employed to calculate the Radon transform and generate the ultrasonic signals. For the inverse problem, the filtered back projection method is chosen to reconstruct the ultrasound sources, which are related to the curl of the current density in the reciprocal process. Based on the curl of the current density in the reciprocal process, four sets of correlation coefficients of the original and reconstructed images' model are all greater than 90%. The uniform error criterion is obtained via multiple reconstructions and comparison of multiple models. The reciprocal model exhibits a good uniformity and stability when describing the actual physical process. It also provides additional effective ideas for solving the inverse problem quickly to reconstruct the ultrasonic sources, which is corresponding to the actual distribution of the conductivity.

**INDEX TERMS** MAET-MI, forward problem, filtered back projection method, reciprocity theorem.

## I. INTRODUCTION

Some surveys show that understanding the electrical properties of biological tissue is very important for the early diagnosis of cancer [1]. Many electrical impedance imaging methods have been proposed for detecting the electrical properties of biological tissues non-invasively, such as Electrical Impedance Tomography (EIT), Magnetoacousto Tomography (MAT), Magnetoacoustic Tomography with Magnetic Induction (MAT-MI) and Magneto-Acousto-Electrical Tomography (MAET) [2]–[8]. EIT is limited by the number of detection sensors and its low spatial resolution. To improve the resolution of biological tissue conductivity images, researchers have studied methods that use a combination of electromagnetic fields and ultrasonic waves such as MAT-MI and MAET [10]–[12]. Even the frequency-modulated ultrasound pulse in MAET is dedicated for simplifying the image signal processing [9]. Guo *et al.* [13] reported that electromagnetic signals can be detected via customized coils in MAET, which is known as Magneto-Acousto-Elect0rical Tomography with Magnetic Induction (MAET-MI). Subsequently, Some scholars used disk multiple layer coils to measure the magnetic field intensity generated [14]. When MAET-MI is compared with MAT-MI [11],

The associate editor coordinating the review of this manuscript and approving it for publication was Avishek Guha.

ultrasound excitation and electromagnetic signal detection steps are employed for the sake of safety; compared to the traditional MAET method that detects signals by electrodes [7], [8], the simple operations of MAT-MI benefits from the separated coils for non-contact detection. Furthermore, compared with EIT and MAT, the resolution of MAET-MI can reach the orders of magnitude of acoustic waves, which is significantly higher than EIT and MAT. The reason for this increase is the introduction of magnetoacoustic. Thus, both EIT and MAT methods need to solve the ill-posedness of the inverse problem, which is an electrical imaging method and not a sound wave based method.

MAET-MI is a conductivity imaging method based on the coupling effect between the electromagnetic field and ultrasound. Transient narrow pulses are emitted sequentially into the target via equispaced ultrasonic transducers around the target. The vibrations of the ultrasound in the target generate distributed currents under the static magnetic field [10]. The distribution of the current varies with ultrasonic propagation, which can be detected via a customized coil. The reconstruction of the relative conductivity distribution can be performed by the current signal, which is detected by the coil.

The reconstruction of electrical conductivity in coil detection mode is the key point in MAET-MI. A set of equations based on the curl of the reciprocal current density is detailed in the forward and inverse problem in MAET-MI. It is necessary to clarify the relationship between the signals detected by the coil and the distribution of the conductivity. Owing to the close relationship between the curl of the reciprocal current density and the conductivity, we put an emphasis on the reconstruction of the curl in inverse problems, rather than reconstructing the conductivity. In the previous work of the MAET-MI, the compressed sensing method was used to reconstruct the curl of current density [9]. A matrix representing the integral was generated to solve the forward problem. The advantage of the compressed sensing method is that it reconstructs images with less data than traditional methods. We reconstruct the curl of the current density by transforming the previous matrix via a compressed sensing method based inverse problem. Forward and inverse problems are all based on the same matrix, which would raise some questions of self-verification. In order to avoid these problems, we solve the forward and the inverse problem via a variety of methods, i.e., the filtered back projection method instead of directly calculating the compressed sensing problem. Both the forward and inverse problems are verified by applying curl of the reciprocal current density, which will be described in future research. In recent studies, Zengin and Lorentz [15] proposed the use of a novel xy coil pair to measure the magnetic field intensity generated due to induced currents. In this paper, circular coil is used to detect the magnetic field intensity generated. This is more conducive to the rapid imaging of axisymmetric model. Moreover, they focus on accurate reconstruction of electrical conductivity through the singular value decomposition. In this paper, the inverse problem of electric field is transformed into the inverse problem of sound field through the derivation of reciprocity theorem. So that the filtered back-projection method can be used to image the model quickly.

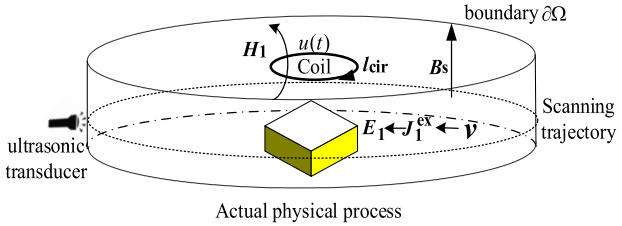


**FIGURE 1.** Actual physical process of MAET-MI.

## II. RECIPROCITY THEOREM

The experimental model of MAET-MI is shown in Figure 1. The actual physical process of and the correspondence between the field variables are marked with arrows. The dotted lines show the placement of the ultrasonic transducers. Its scanning trajectory, which emits ultrasonic waves into the imaging area $\Omega$ from the boundary $\partial\Omega$. The vibration velocity $\gamma$ excites the dynamic source current density $J_1^{ex}$ in the static magnetic field, which corresponding to equation (1) below.

$$\boldsymbol{J}_1^{\boldsymbol{ex}} = \sigma \boldsymbol{\gamma} \times \boldsymbol{B}_s, \tag{1}$$

where $\sigma$ is a parameter that is infinitely close to zero but not zero. The $B_s$ is static magnetic field.

An induced electric field $E_1$ and a varying magnetic field $H_1$ are generated under the excitation of $J_1^{ex}$. Since $E_1$ and $H_1$ vary with the propagation of sound waves, voltage $u(t)$ is induced in the coil, where t represents time.

In the coil detection method, the relationship between the magnetic field and the electric field can be described by Faraday's law of electromagnetic induction Eq. (2a) and Ampere's law Eq. (2a).

$$\nabla \times \boldsymbol{E}_1 = -\mu \frac{\partial \boldsymbol{H}_1}{\partial t}, \tag{2a}$$

$$\nabla \times \boldsymbol{H}_1 = \boldsymbol{J}_1^{ex} + \sigma \boldsymbol{E}_1, \tag{2b}$$

where subscript 1 indicates the field in the actual physical process. $H_1$ is the total magnetic field intensity in the target area. $J_1^{ex}$ is the dynamic source current density caused by the ultrasound vibration, and $u$ is the dielectric permeability, where $\nabla$ is a gradient operator, expressed in Cartesian coordinates as $\nabla = \frac{\partial}{\partial x}\mathbf{e}_x + \frac{\partial}{\partial y}\mathbf{e}_y + \frac{\partial}{\partial z}\mathbf{e}_z$. Since the electric field $E_1$ has a vortex component, the induced voltage can be detected by a coil according to the electromagnetic induction. The induced voltage in the coil can be expressed as the following line integral.

$$u(t) = \int_{r \in \boldsymbol{l}_{cir}} \boldsymbol{E}_1 \cdot d\boldsymbol{l}_{cir}, \tag{3}$$

where $dl_{cir}$ represents a tiny line element along the detection coil.

By dividing the conductivity of the right side of Eq. (2b) to the left side and calculate the curl at both ends. Then combine Eq. (1) and Eq. (2a) to obtain

$$\nabla \times (\frac{1}{\sigma}\nabla \times \boldsymbol{H}_1) + \mu \frac{\partial \boldsymbol{H}_1}{\partial t} = \nabla \times (\boldsymbol{\gamma} \times \boldsymbol{B}_s). \tag{4}$$

Eq. (4) is a vector field equation that can be solved by the given boundary. The numerical solution of Eq. (4) can be determined by using the finite element method with an infinite boundary condition. By calculating the Eq. (4), we found the magnetic field intensity $H_1$, and put it into Eq. (2), then we can calculate the electric field intensity. This is also a direct coupling calculation method for computing the forward problem of MAET-MI.

Figure 2 shows the reciprocal process of MAET-MI and the corresponding field variables. In the same problem area, as shown in Fig.1, a time-varying current density, $J_2^{ex}$ , is switched into the coil. The eddy current density, $J_2$, and the electric field, $E_2$, are induced in the target.

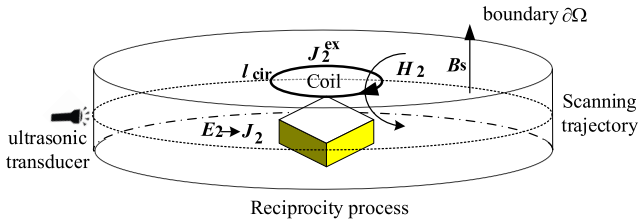


**FIGURE 2.** Corresponding reciprocal process.

The reciprocity theorem of MAET-MI is to provide the coil with a pulsed current and to induce an eddy current distribution in the target. We assume that the detection coil is a line loop with a section area of $\boldsymbol{0}$. The applied current density can be expressed as follows:

$$\boldsymbol{J}_2^{ex} = \delta^3(\boldsymbol{r} - \boldsymbol{r}_{cir}) f(t) \boldsymbol{l}_{\boldsymbol{cir}}(\boldsymbol{r}). \tag{5}$$

Of which $r$ represents the field point in $\Omega$, $r_{cir}$ represents the point on the coil, $\delta(\cdot)$ represents the Dirac function in three-dimensional space, $f(t)$ is the time term of the applied current $J_2^{ex}$, $l_{cir}$ represents the unit vector of $J_2^{ex}$ along the circumferential direction of the coil. According to the selectivity of the Dirac function, $\delta^3(r - r_{cir})$ denotes that the applied current density $J_2^{ex}$ is applied only to the coil and has no value elsewhere.

Similarly, according to the Ampere Law and Faraday Law of electromagnetic induction, the electric and magnetic fields excited by an applied current in the reciprocity theorem can be expressed as

$$\nabla \times \boldsymbol{E}_2 = -\mu \frac{\partial \boldsymbol{H}_2}{\partial t} \tag{6a}$$

$$\nabla \times \boldsymbol{H}_2 = \boldsymbol{J}_2^{ex} + \sigma \boldsymbol{E}_2 \tag{6b}$$

Here subscript 2 denotes the field in the reciprocity theorem. $E_2$ and $H_2$ are eddy electric field and magnetic field respectively. The displacement current is neglected because of the low excitation frequency.

Make Inner product between Eq.(2b) and $E_2$, we obtain.

$$\iiint_{r\in\Omega} \nabla \times \boldsymbol{H}_1 \cdot \boldsymbol{E}_2 d\Omega = \iiint_{r\in\Omega} \boldsymbol{J}_2^{ex} \cdot \boldsymbol{E}_2 d\Omega + \iiint_{r\in\Omega} \sigma \boldsymbol{E}_1 \cdot \boldsymbol{E}_2 d\Omega \tag{7}$$

$\Omega$ is the whole computational region, which includes the target region and the coil.

According to the vector identical equation

$$\nabla \cdot (A \times B) = B \cdot \nabla \times A - A \cdot \nabla \times B, \tag{8}$$

where A and B are variables in the vector identical equation. The left-hand side of Eq. (7) can be rewritten to

$$\iiint_{r\in\Omega} \nabla \times \boldsymbol{H}_1 \cdot \boldsymbol{E}_2 d\Omega = \iiint_{r\in\Omega} \nabla \times \boldsymbol{E}_2 \cdot \boldsymbol{H}_1 d\Omega - \iiint_{r\in\Omega} \nabla \cdot (\boldsymbol{E}_2 \times \boldsymbol{H}_1) d\Omega \tag{9}$$

Applying the Gauss theorem to the Eq. (9), it can be simplified to

$$\begin{aligned} &\iiint_{r\in\Omega} \nabla \times \boldsymbol{H}_1 \cdot \boldsymbol{E}_2 \boldsymbol{d}\Omega \\ &= \iiint_{r\in\Omega} \nabla \times \boldsymbol{E}_2 \cdot \boldsymbol{H}_1 d\Omega - \iiint_{r\in\partial\Omega} (\boldsymbol{E}_2 \times \boldsymbol{H}_1) \cdot \boldsymbol{n} d\partial\Omega \\ &= -\iiint_{r\in\Omega} \mu \frac{\partial \boldsymbol{H}_2}{\partial \boldsymbol{t}} \cdot \boldsymbol{H}_1 \boldsymbol{d}\Omega, \end{aligned} \tag{10}$$

where $\mu$ is the permeability of the medium. $\boldsymbol{n}$ represents the unit vector in the exterior normal direction of the boundary. When the solution region is large enough, $E_2$ is zero at the boundary under infinite boundary conditions, and thus the boundary integral of $(E_2 \times H_1) \times n$ is also zero [16]. By taking into account Eq. (10), Eq. (9) can be rewritten as

$$-\iiint_{r\in\Omega} \mu \frac{\partial \boldsymbol{H}_2}{\partial t} \cdot \boldsymbol{H}_1 d\Omega = \iiint_{r\in\Omega} \boldsymbol{J}_1^{ex} \cdot \boldsymbol{E}_2 d\Omega + \iiint_{r\in\Omega} \sigma \boldsymbol{E}_1 \cdot \boldsymbol{E}_2 d\Omega. \tag{11}$$

Similarly, both sides of Eq. (9b) can produce scalar product of $E_1$.

$$-\iiint_{r\in\Omega} \mu \frac{\partial \boldsymbol{H}_1}{\partial t} \cdot \boldsymbol{H}_2 d\Omega = \iiint_{r\in\Omega} J_2^{ex} \cdot \boldsymbol{E}_1 d\Omega + \iiint_{r\in\Omega} \sigma \boldsymbol{E}_2 \cdot \boldsymbol{E}_1 \boldsymbol{d}\Omega. \tag{12}$$

The frequency domain expressions are found by taking the Fourier transform of both sides of Eq. (11) and Eq. (12).

$$-\iiint_{r\in\Omega} j\omega \mathring{\boldsymbol{H}}_2 \cdot \mathring{\boldsymbol{H}}_1 \, d\Omega = \iiint_{r\in\Omega} \mathring{J}_1^{ex} \cdot \mathring{\boldsymbol{E}}_2 \, d\Omega + \iiint_{r\in\Omega} \sigma \mathring{\boldsymbol{E}}_1 \cdot \mathring{\boldsymbol{E}}_2 \boldsymbol{d}\Omega \tag{13a}$$

$$-\iiint_{r\in\Omega} j\omega \overset{\circ}{\boldsymbol{H}}_1 \cdot \overset{\circ}{\boldsymbol{H}}_2 \, d\Omega = \iiint_{r\in\Omega} \overset{\circ}{J}_2^{x} \cdot \overset{\circ}{\boldsymbol{E}}_1 \, d\Omega + \iiint_{r\in\Omega} \sigma \overset{\circ}{\boldsymbol{E}}_2 \cdot \overset{\circ}{\boldsymbol{E}}_1 \, d\Omega, \quad (13b)$$

where $\boldsymbol{j}$ is an imaginary number unit. The o above the variable represents the corresponding field in the frequency domain. This can be easily established as

$$\iiint_{r\in\Omega} \overset{\circ}{J}_1^{ex} \cdot \overset{\circ}{\boldsymbol{E}}_2 \, d\Omega = \iiint_{r\in\Omega} \overset{\circ}{J}_2^{ex} \cdot \overset{\circ}{\boldsymbol{E}}_1 \, \boldsymbol{d}\Omega \quad (14)$$

The variables in Eq. (14) are functions of space location $\boldsymbol{r}$ and the angular frequency $\omega$, they can be expressed in detail via the characterization below

$$\iiint_{r\in\Omega} \overset{\circ}{J}_1^{ex}(r,\omega) \cdot \overset{\circ}{E}_2(r,\omega)\, d\Omega = \iiint_{r\in\Omega} \overset{\circ}{J}_2^{ex}(r,\omega) \cdot \overset{\circ}{E}_1(r,\omega)\, d\Omega \quad (15)$$

Next, we replace the Eq. (1) with the left part of Eq. (15). Then, according to $\overset{\circ}{J}_2 = \sigma \overset{\circ}{E}_2$, we can obtain

$$\iiint_{r\in\Omega} \overset{\circ}{J}_1^{ex}(r,\omega) \cdot \overset{\circ}{E}_2(r,\omega)\, d\Omega = \iiint_{r\in\Omega} \overset{\circ}{J}_2^{ex}(r,\omega) \cdot \left[\overset{\circ}{\gamma}(r,\omega) \times B_s\right] d\Omega. \quad (16)$$

By combining Eq. (3) and Eq. (8), then Eq. (15) can be transformed to

$$\begin{aligned}
&\iiint_{r\in\Omega} \overset{\circ}{J}_2^{ex}(r,\omega) \cdot \overset{\circ}{E}_1(r,\omega)\, d\Omega \\
&= \iiint_{r\in\Omega} \overset{\circ}{E}_1(r,\omega) \cdot \hat{n}(r)\, \delta^3(r - r_{cir}) \overset{\circ}{f}(\omega)\, d\Omega \\
&= \int_{r\in l_{cir}} \overset{\circ}{S}(\omega) \overset{\circ}{E}_1(r,\omega) \cdot dl_{cir} \\
&= \overset{\circ}{u}(\omega) \overset{\circ}{f}(\omega), \quad (17)
\end{aligned}$$

where $\overset{\circ}{S}(\omega)$ and $\overset{\circ}{u}(\omega)$ are Fourier transforms of $s(t)$ and $u(t)$, respectively, and $s(t)$ is the time term of the applied current $J_2^{ex}$. $\overset{\circ}{f}(\omega)$ and $\overset{\circ}{u}(\omega)$ are Fourier transforms of $f(t)$ and $u(t)$ respectively. As shown in Eq. (17), the Dirac function converts the volume fraction of the three-dimensional space into a line integral along the coil. According to Eq. (15) - Eq. (17), the frequency domain expression of the induced voltage detected by the coil is

$$\overset{\circ}{u}(\omega) \overset{\circ}{f}(\omega) = \iiint_{r\in\Omega} \overset{\circ}{J}_2(r,\omega) \cdot \left[\overset{\circ}{\gamma}(r,\omega) \times \boldsymbol{B}_s\right] d\Omega \quad (18)$$

The right part of Eq. (18) is similar to the expression of the electrode detection mode deduced by [5]–[7]. Except that the static magnetic field $B_s$ is frequency independent, such that all field quantities are functions of angular frequency $\omega$ and space point $r$.

Now, by considering Gauss' theorem, Eq. (8) and the velocity potential function

$$\gamma = \frac{1}{\rho_0} \nabla \phi, \quad (19)$$

where $\phi$ is the velocity potential function. $\rho_0$ is the static density of the medium. Eq. (18) can be rewritten as

$$\begin{aligned}
&\overset{\circ}{u}(\omega) \overset{\circ}{f}(\omega) \\
&= \iiint_{r\in\Omega} \frac{\boldsymbol{B_0}}{\rho_0} \cdot \nabla \times \overset{\circ}{\boldsymbol{J_2}}(r,\omega) \overset{\circ}{\phi}(r,\omega)\, d\Omega \\
&\quad - \int\int_{r\in\partial\Omega} \overset{\circ}{\boldsymbol{J_2}}(r,\omega) \times \frac{\boldsymbol{B_s}}{\rho_0} \overset{\circ}{\phi}(r,\omega)\, d\partial\Omega, \quad (20)
\end{aligned}$$

where $\overset{\circ}{\varphi}(r,\omega)$ is Fourier transform of $\phi(r,t)$. Eq. (20) is split into two components: an individual integral and a surface integral. For simplicity, if the target is enclosed in a non-conductive insulating fluid medium, such as insulating oil or distilled water, the current density at the boundary is zero in the reciprocity theorem. Therefore, the second boundary integral on the right side of Eq. (20) is 0. Considering the acoustic homogeneous medium, Eq. (20) can be simplified to

$$\overset{\circ}{u}(\omega) \overset{\circ}{f}(\omega) = \frac{1}{\rho_0} \iiint_{r\in\Omega} \boldsymbol{B_s} \cdot \nabla \times \overset{\circ}{\boldsymbol{J_2}}(r,\omega) \overset{\circ}{\phi}(r,\omega)\, d\Omega \quad (21)$$

Because of the target's low conductivity, the induced eddy current is approximately the same at each point, regarded as the temporal term. This means that time and space terms of induced eddy currents can be separated according the conductivity of objects. Spatial and frequency terms can also be separated. Therefore,

$$\overset{\circ}{\boldsymbol{J_2}}(r,\omega) = \overset{\circ}{\boldsymbol{J_2}}(r) \overset{\circ}{\boldsymbol{F}}(\omega). \quad (22)$$

$\overset{\circ}{J}_2(r)$ and $\overset{\circ}{F}(\omega)$ respectively denote the space and time terms of the induced eddy current in the reciprocity theorem. The temporal term of an induced electric field, or current, should be the first derivative of the temporal term of the induced magnetic field $H_2$. Therefore, in the frequency domain, $\overset{\circ}{\boldsymbol{F}}(\omega)$ should be

$$\overset{\circ}{F}(\omega) = j\omega \overset{\circ}{f}(\omega) \quad (23)$$

By considering Eq. (22) and Eq. (23), Eq. (21) can be rewritten as

$$\overset{\circ}{u}(\omega) \overset{\circ}{f}(\omega) = \overset{\circ}{f}(\omega) \frac{1}{\rho_0} \iiint_{r\in\Omega} \boldsymbol{B_s} \cdot \nabla \times \overset{\circ}{\boldsymbol{J_2}}(r)\, j\omega \overset{\circ}{\phi}(r,\omega)\, d\Omega. \quad (24)$$

If we assume that $\overset{\circ}{f}(\omega)$ is a constant, then $f(t)$ is equal to $\delta^3(t)$ and $\overset{\circ}{u}(\omega)$ can be simplified to

$$\overset{\circ}{u}(\omega) = \frac{1}{\rho_0} \iiint_{r\in\Omega} \boldsymbol{B_s} \cdot \nabla \times \overset{\circ}{\boldsymbol{J_2}}(r)\, j\omega\, \overset{\circ}{\phi}(r,\omega)\, d\Omega. \quad (25)$$

Generally speaking, as long as $\overset{\circ}{f}(\omega)$ is non-zero in the non-zero frequency spectrum of $\overset{\circ}{u}(\omega)$, the expression can be reduced to Eq. (25). In MAET-MI, $\overset{\circ}{f}(\omega)$ is decided by actual physical process. Montalibet *et al.* [10] assumed that $s$(t) is a step function, which is equivalent to assuming $\overset{o}{f}(\omega) = \pi\delta(\omega) + \frac{1}{j\omega}$. However, as long as $\overset{\circ}{f}(\omega)$ has no zero value in the non-zero spectrum range of $\overset{\circ}{u}(\omega)$, $\overset{\circ}{f}(\omega)$ can be selected as the excitation in the reciprocity theorem and be removed. For simplicity, we choose $f(t) = \delta(t)$, which is equivalent to $\overset{\circ}{f}(\omega) = 1$. Eq. (25) also illustrates that the MAE signal is related to the spatial component of curl of current density in the reciprocal process.

If the inverse Fourier transform is used in Eq. (25), the time domain integral expression can be obtained as follows:

$$u(t) = \frac{1}{\rho_0} \iiint_{\boldsymbol{r}\in\Omega} \boldsymbol{B}_s \cdot \nabla \times \boldsymbol{J}_2^o(\boldsymbol{r})\varphi'(\boldsymbol{r},t) d\Omega \quad (26)$$

Among them, $\varphi'(r,t)$ represents the first temporal derivative of the velocity potential function $\varphi(r,t)$. Substitute Eq. (22) and Eq. (23) into Eq. (18), reduce $\overset{\circ}{f}(\omega)$ on both sides and solve inverse Fourier transform, and then the time domain integral expression can be obtained

$$u(t) = \iiint_{\boldsymbol{r}\in\Omega} \overset{\circ}{\boldsymbol{J}}_2(\boldsymbol{r}) \cdot \boldsymbol{\gamma'}(\boldsymbol{r},t) \times \boldsymbol{B}_s d\Omega \quad (27)$$

From the above, the induced voltage signal can also be obtained by the reciprocity theorem via forward problem. Eq. (25) is based on reciprocal current density curl in coil detection mode, while Eq. (27) is based on the reciprocal current density in the coil detection mode. Since $\boldsymbol{\gamma'}(\boldsymbol{r},t)$ is the derivative of the vibration velocity ($\boldsymbol{\gamma}(\boldsymbol{r},t)$), the distribution of the vibration velocity is a spherical surface under impulse excitation. Therefore, Eq. (27) can be converted into a spherical integral. Then, the integral equation can be solved by a Radon transform and generated by the ultrasonic signals. Based on the reciprocity theorem, we can transform the measurement of electrical signals into solving the wave equation. And then reconstruct the curl of current density via filtered back projection, which has robustness. This is different from our previous work, where we finished reconstructing the curl of current density of the inverse problem of MAET-MI with the filtered back projection method instead of the compressed sensing method. Reconstruction of the current density and reconstruction of conductivity are closely related. Details about the subsequent reconstruction steps can be found in the references of other scholars [11].

## III. INVERSE PROBLEM

According to the formulas in section II, the MAET-MI inverse problem could be divided into two steps. First, solve the integral in Eq. (27). Second, reconstruct conductivity with respect to the space of the reciprocal current density or its curl.

Then, the integral in Eq. (26) can be regarded as the solution of the following MAET based wave equation.

$$\nabla^2 u - \frac{1}{v_s^2}\frac{\partial^2 u}{\partial t^2} = -H(\boldsymbol{r'})\delta'(t), \quad (28)$$

where $v_s$ is the velocity of ultrasonic vibration. The field of wave equation $u(r,t)$ is excited by any wave field source $H(r')$ with excitation $\delta'(t)$. Under infinite boundary conditions, the solution of the wave equation can be expressed as an integral of the derivative of the Green's function

$$u(\boldsymbol{r},t) = \iiint_{\boldsymbol{r'}\in\Omega} H(\boldsymbol{r'})G'(\boldsymbol{r},t|\,\boldsymbol{r'},0)d\Omega, \quad (29)$$

where $r'$ represents the source point, $\boldsymbol{r}$ represents the field point, and $H(r')$ represents the field source distribution function. $G(r,t|\,r',0)$ represents the Green function of point source excitation field $u(r,t)$, which still satisfies

$$\nabla^2 G - \frac{1}{v_s^2}\frac{\partial^2 G}{\partial t^2} = -\delta(t)\delta^3(\boldsymbol{r}-\boldsymbol{r'}). \quad (30)$$

Setting the wave field source to

$$H(\boldsymbol{r'}) = \nabla \times \overset{\circ}{\boldsymbol{J}}_2(\boldsymbol{r'}) \cdot \boldsymbol{B_S}/\rho_0, \quad (31)$$

the inverse problem of MAET-MI based coil detection can still be transformed into the inverse source reconstruction problem of wave Eq. (28), in which the distribution source satisfies the Eq. (31) [17].

The filtered back projection method can be used to reconstruct the curl of the current density. The Hilbert transformation formula is used in the reconstruction of the current density by using filtered back projection [16]

$$\varphi(r) \approx \frac{C}{\beta I_0 v_s^2} \oint ds \frac{n\cdot(r-r_\theta)}{|(r-r_\theta)|^2} H(p_1(r_\theta, |(r_\theta - r)|/v_s) \times |(r-r_\theta)| + p_2(r_\theta, |(r_\theta - r)|/v_s)), \quad (32)$$

where $\boldsymbol{H}$ is a Hilbert transform; $p_2(r,t) = v_s \int_0^t p_2(r,t)dt$, $\boldsymbol{n}$ is the inward normal to the detection curve at $r_\theta$, $\boldsymbol{ds}$ is the arc length differential, and the integration is along a complete detection curve (the curve that runs around the object-of-interest).

## IV. NUMERICAL RESULTS

To fully exemplify the advantages and feasibility of the forward model in the reciprocity theorem, we vary the diameter and position of the model to reconstruct the conductivity distribution.

First, the forward simulation of the MAET-MI is performed. The schematic diagram of the final physical model is shown in Fig.3.

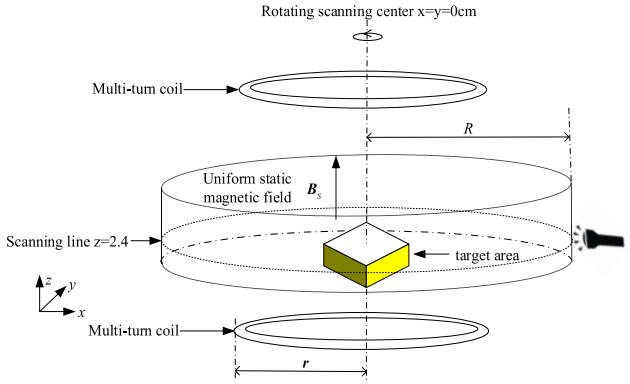


**FIGURE 3.** Schematic diagram of coil Magneto-Acousto-Electro imaging model.

The multilayer cylindrical object in the center is the object to be imaged. A multi-turn detection coil is placed on each side of the area to be imaged. The imaging body and coil are placed in the static magnetic field with magnetic induction of $B_s$, and the diameter for the inner circle of the coil is 1 cm. The ultrasonic transducer transmits the ultrasonic wave to the target body and rotates along the dotted line for scanning. Similarly, we adopt the two-dimensional model of ultrasound tomography and find that when the image area is small enough along the z-direction, only a two-dimensional plane (at z = 2.4 cm) is approximately considered for simplicity.

The two-dimensional conductivity distribution of the model is shown in Fig. 4(a), which is a square area with 6 cm length. It includes two concentric circular conductivity anomalies body in the diameters of 5 cm and 10 cm respectively. The background conductivity is 0 S/m, and the two anomalies are 1 S/m inside and 0.1 S/m outside. As shown in Fig. 4(b), by changing the conductivity, the conductivity distribution of the two-dimensional cross-section is constructed using a 0.2 S/m inside and a 0.3 S/m outside. We only increase the radius of the middle circle without changing the conductivity. Then, we obtain the conductivity distribution of the two-dimensional cross-section, as shown in Fig. 4(c). The model shown in Fig. 4(a) establishes a three-layer concentric circular conductivity anomaly volume model with internal and external conductivities of 0.2 S/m, 1 S/m and 0.1 S/m from inside to outside. The two-dimensional cross-sectional conductivity distribution is shown in Fig. 4(d).

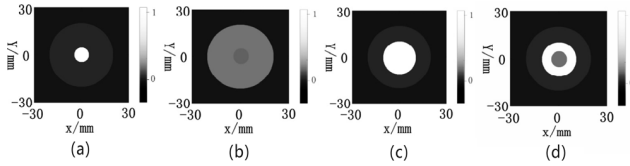


**FIGURE 4.** Conductivity distribution corresponding to four different models.

Under the given ultrasound excitation, the Magneto-Acousto-Electric (MAE) signals are calculated by a direct multiphysics coupling method and the reciprocity theorem, respectively. The results are illustrated as follows in this section.

The normalized MAE signals calculated by the two methods are shown in Fig. 5 (a), (b), (c) and (d). The blue line represents the signals calculated directly by the finite element method (FEM), and the red dotted line represents the signals calculated by the integral equation based reciprocity theorem. The FEM method determines the grid size and other model parameters. It is easy to achieve convergence when the grid size is 1/6 the wavelength.

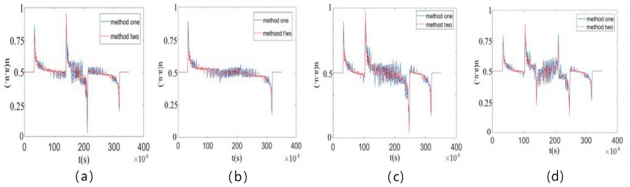


**FIGURE 5.** Contrast images of MAE signals of four different models.

By comparing the results, we can see that the results calculated using the integral equation of the reciprocity theorem are consistent with counterparts calculated directly by the FEM, and a similar result is found for the waveform. This proves the validity of reciprocity theorem for MAET-MI and validates the results calculated by integral Eq. (26) or Eq. (27). Although the current density curl does not fully characterize the conductivity, Figure 4 and Figure 5 shows that the curves are substantially similar. Therefore, the distribution of conductivity can be inferred by observing the current density rotation.

The conductivity distribution of the two-dimensional cross-section of the four different models discussed in this section is shown in Figs. 4(a), (b), (c) and (d). The curl of the current density, a reciprocal process, is shown in Fig. 6 (a), (b), (c), and (d). The curl of current density is reconstructed via the filtered back projection method based on the surrounding MAE signals, which is shown in Fig.7 (a), (b), (c) and (d).

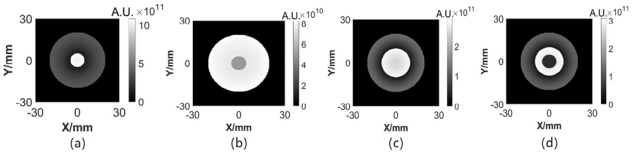


**FIGURE 6.** Curl contrast images from forward modeling of reciprocal processes of four different models.

In Figs. 4, 6, 7, the curl of the current density varies greatly with the interface of conductivity. A numerical variable $T$ is introduced to the following formula (Eq. (33)) to measure the correlation between the original model and the reconstructed image.

$$T = \frac{\sum (\mathbf{A}_{ij} \times \mathbf{B}_{ij})}{\sqrt{\sum (\mathbf{A}_{ij} \times \mathbf{A}_{ij})} \times \sqrt{\sum (\mathbf{B}_{ij} \times \mathbf{B}_{ij})}} \tag{33}$$

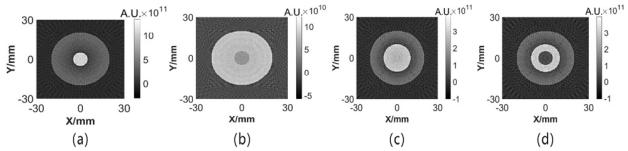


**FIGURE 7.** Curl contrast images of ultrasound signal reconstruction of four different models.

The A represents the pixel matrix of the original image and B represents the pixel matrix of the reconstruction image. The T terms the correlation coefficients between the original and reconstructed images. The four sets of correlation coefficients are 91.50%, 95.75%, 93.98% and 91.05%. By comparison, we find that the curl of the current density obtained by the finite element method (FEM) based on the reciprocal process is almost the same as that of the current density reconstructed from the MAE signals. The similarity of the four models was greater than 90%. We obtain similar images that are reconstructed by using different numerical models. The error is obtained by using multiple reconstruction methods and by comparing multiple models. We find that the reciprocal model exhibits good uniformity and stability when describing the actual physical process. Thus, we verify that the reconstruction method based on the electrode detection can be applied to MAET-MI. Thus, the inverse MAET-MI problem can be transformed into an inverse source reconstruction of the wave equation based on the coil detection.

## V. CONCLUSION

In summary, starting from the actual physical process of MAET-MI, we first study the reciprocity theorem under coil detection mode. A variety of approaches are adopted to calculate the forward and the inverse problems. This is done to verify the reciprocal model. In the forward problem, the moment method is employed to calculate the Radon transform to generate the ultrasonic signals. For the inverse problem, the filtered back projection method is chosen to reconstruct the ultrasound sources, which are related to the curl of the current density in the reciprocal process. By applying the curl of the current density to the reciprocal process and by comparing the reconstructed and directly calculated methods, we find that the reconstruction of the current density curl is consistent with the results obtained by the FEM. All the simulation results support the reasonability of the reciprocal algorithm and verify its effectiveness. This not only proves the correctness of the reciprocal models, but also provides a different effective idea for solving the inverse problem by reciprocity theorem and provides a method for imaging conductivity quickly.

## REFERENCES

[1] Y. Zou and Z. Guo, "A review of electrical impedance techniques for breast cancer detection," *Med. Eng. Phys.*, vol. 25, no. 2, pp. 79–90, 2003.
[2] H. Wen, J. Shah, and R. S. Balaban, "Hall effect imaging," *IEEE Trans. Biomed. Eng.*, vol. 45, no. 1, pp. 119–124, Jan. 1998.
[3] S. Haider, A. Hrbek, and Y. Xu, "Magneto-acousto-electrical tomography: A potential method for imaging current density and electrical impedance," *Physiol. Meas.*, vol. 29, no. 6, pp. S41–S50, 2008.
[4] L. Kunyansky, "Reconstruction of a function from its spherical (circular) means with the centers lying on the surface of certain polygons and polyhedra," *Inverse Problems*, vol. 27, no. 2, 2011, Art. no. 025012.
[5] L. Kunyansky, "Fast reconstruction algorithms for the thermoacoustic tomography in certain domains with cylindrical or spherical symmetries," *Inverse Problems Imag.*, vol. 6, no. 1, pp. 111–131, 2017.
[6] L. Kunyansky and P. Kuchment, "Synthetic focusing in ultrasound modulated tomography," in *Proc. Workshop Math. Algorithms Tomogr.*, 2010, pp. 44–47.
[7] Z. Yu, S. Dai, Q. Ma, G. Guo, J. Tu, and D. Zhang, "Conductivity anisotropy influence on acoustic sources for magnetoacoustic tomography with magnetic induction," *IEEE Trans. Biomed. Eng.*, vol. 65, no. 11, pp. 2512–2518, Nov. 2018.
[8] Y. Zhou, Q. Ma, G. Guo, J. Tu, and D. Zhang, "Magneto-acousto-electrical measurement based electrical conductivity reconstruction for tissues," *IEEE Trans. Biomed. Eng.*, vol. 65, no. 5, pp. 1086–1094, May 2017.
[9] Y. Li, G. Liu, H. Xia, and Z. Xia, "Numerical simulations and experimental study of magneto-acousto-electrical tomography with plane transducer," *IEEE Trans. Magn.*, vol. 54, no. 3, Mar. 2018, Art. no. 5100704.
[10] A. Montalibet, J. Jossinet, A. Matias, and D. Cathignol, "Electric current generated by ultrasonically induced Lorentz force in biological media," *Med. Biol. Eng. Comput.*, vol. 39, no. 1, pp. 15–20, 2001.
[11] Y. Xu and B. He, "Magnetoacoustic tomography with magnetic induction (MAT-MI)," *Phys. Med. Biol.*, vol. 50, no. 21, pp. 5175–5187, 2005.
[12] Y. Xu, L. V. Wang, G. Ambartsoumian, and P. Kuchment, "Reconstructions in limited-view thermoacoustic tomography," *Med. Phys.*, vol. 31, no. 4, pp. 724–733, 2004.
[13] L. Guo, G. Liu, and H. Xia, "Magneto-acousto-electrical tomography with magnetic induction for conductivity reconstruction," *IEEE Trans. Biomed. Eng.*, vol. 62, no. 9, pp. 2114–2124, Sep. 2015.
[14] K. Kaboutari, A. Ö. Tetik, and E. Ghalichi, "Data acquisition system for MAET with magnetic field measurements," *Phys. Med. Biol.*, vol. 64, no. 11, 2019, Art. no. 115016.
[15] R. Zengin and N. G. Gençer, "Lorentz force electrical impedance tomography using magnetic field measurements," *Phys. Med. Biol.*, vol. 61, no. 16, p. 5887, 2016.
[16] V. S. Vladimirov, *Equations of Mathematical Physics: Pure and Applied Mathematics*, vol. 3, A. Jeffrey, Ed. New York, NY, USA: Marcel Dekker, 1971.
[17] A. M. Stewart, "Longitudinal and transverse components of a vector field," 2008, *arXiv:0801.0335*. [Online]. Available: https://arxiv.org/abs/0801.0335

**LIKUN GONG** was born in Weihai, Shandong, China, in 1998. He received the degree from the China University of Petroleum.

His research interests include inverse problems, multiphysical field coupling, and magnetoacoustic imaging.

Mr. Gong awards and honors include the National Endeavor Fellowship and the Science and Technology Innovation Scholarship from the China University of Petroleum, East China.

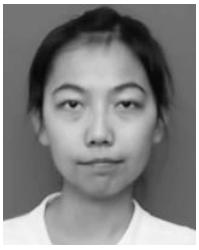

**LAN YANG** was born in Xinjiang, China, in 1997. She received the degree from the China University of Petroleum.

Her research interests include inverse problems, multiphysical field coupling, and magnetoacoustic imaging.

Ms. Yang received the School Scholarship, School-Level Scholarship, and Social Work Scholarship from the China University of Petroleum, East China.

**SIYI YANG** was born in Zhangjiakou, Hebei, China, in 1998. She received the degree from the China University of Petroleum, in 2016.

Her research interests include inverse problems, multiphysical field coupling, and magnetoacoustic imaging. She has a national innovation and entrepreneurship project for college students and a training program for college students of the Chinese Academy of Sciences.

Ms. Yang awards and honors include the Honorary Titles of Excellent Students and the Comprehensive Excellent Scholarship from the China University of Petroleum.

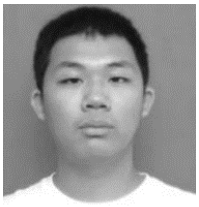

**YUANZE WANG** was born in Dongying, Shandong, China, in 1997. He received the degree from the China University of Petroleum, in 2016.

His research interests include circuit designing, circuit modeling, signal processing, and embedded programming.

Mr. Wang awards and honors include the 1st prize of National Undergraduate Electronic Designing Contest, Outstanding Contribution, and the Science and Technology Innovation Scholarship from the China University of Petroleum, East China.

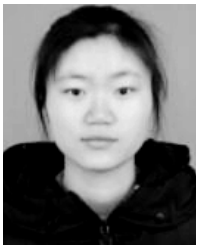

**MINJING ZHONG** is currently pursuing the master's degree with the College of Information and Control Engineering, China University of Petroleum, Qingdao, China. Her current research interest includes electromagnetic inverse scattering problem.

**LIANG GUO** received the B.E. and M.E. degrees in electronic engineering and control theory and engineering from the China University of Petroleum, Shandong, China, in 2002 and 2005, respectively. He is currently pursuing the Ph.D. degree with the Institute of Electrical and Electricity, China Academy of Sciences, Beijing, China. From 2005 to 2012, he was a Lecturer with the China University of Petroleum. His current research interests include the computation of coupled field, medical imaging, process tomography, weak signal detection, and circuit design.